Геология и геофизика, т. 65, № 11, с. 1609—1620, DOI: 10.15372/GiG2024126, EDN: READJJ
Поступила в редакцию 19.09.2024, принята в печать 21.05.2024

УДК 550.360+552.52

ГЕОТЕРМОМЕТРИЯ ИЛЛИТИЗАЦИИ СМЕКТИТА НЕФТЕГАЗОМАТЕРИНСКИХ ПОРОД ВЕРХНЕГО БАССЕЙНА ИНДА (*Пакистан*)

А. Али, С. Уллах

Университет Пешавара, Пешавар 25120, Хайбер-Пахтунхва, Пакистан

Метод геотермии применялся при изучении иллитизации смектита для оценки термической зрелости и углеводородного потенциала позднепалеоценовой–раннеэоценовой формации Патала в верхнем бассейне Инда. Рентгеноструктурный анализ выявил в ее отложениях иллит, мусковит, кварц, каолинит, хлорит и кальцит. Сравнение дифракционных рентгенограмм воздушно-сухих и этиленгликоль-сольватированных образцов отложений показало отсутствие дискретного смектита и переслаивающегося иллит-смектита. Кроме того, присутствие аутигенного иллита $2M_1$ указывает на то, что формация Патала является частью зоны поздней стадии диагенеза (нижней анхизоны), которая расположена в зоне иллитизации R3. Высокое содержание SiO_2 и Al_2O_3 в глинистой фракции формации Патала указывает на замещение тетраэдрического Si^{4+} на Al^{3+} в прослоях смектита. Аналогично высокое содержание K_2O относительно CaO и MgO свидетельствует о замещении K^+ на Ca^{2+} и Mg^{2+} в процессе иллитизации смектита. Сканирующая электронная микроскопия показала локальный рост пластинчатых кристаллов иллита, образующихся в зоне R3. Помимо этого, общее содержание органического углерода в сланцах формации Патала, обнажающихся в районе Тираха, позволяет судить о низком или высоком генерационном потенциале нефтегазоматеринских пород. Отсутствие дискретного смектита и иллит-смектита, а также выявление дискретного иллита в сланцах формации Патала, вероятно, указывают на то, что углеводороды могли мигрировать из нефтегазоматеринских пород в породы-коллекторы в процессе иллитизации смектита.

Иллитизация смектита, геотермометрия, зона R3, формация Патала, верхний бассейн Инда

SMECTITE ILLITIZATION GEOTHERMOMETRY OF THE UPPER INDUS BASIN HYDROCARBON SOURCE ROCKS (*Pakistan*)

A. Ali, S. Ullah

Smectite illitization geothermometry has been used to assess the thermal maturity and hydrocarbon generation potential of the late Paleocene to early Eocene Patala Formation in the Upper Indus Basin. X-ray diffraction (XRD) detected illite, muscovite, quartz, kaolinite, chlorite, and calcite. Comparison between air-dried (AD) and ethylene glycol (EG)-solvated XRD patterns reveals the absence of discrete smectite and interstratified illite-smectite (I-Sm). Additionally, authigenic illite-$2M_1$ indicates that the Patala Formation has entered the late-stage diagenetic zone or the low anchizone, which lies in the R3 illitization zone. Abundant SiO_2 and Al_2O_3 in the Patala clay fraction indicate the substitution of tetrahedral Si^{4+} by Al^{3+} within the smectite interlayers. Likewise, the relative abundance of K_2O to CaO and MgO indicates the exchange of K^+ with Ca^{2+} and Mg^{2+} during smectite illitization. Scanning electron microscopy (SEM) reveals in situ growth of platy illite crystals that form within the R3 zone. Furthermore, the total organic carbon (TOC) of the Patala shale exposed in Tirah suggests a poor to good source rock. The absence of discrete smectite and I-Sm, combined with the detection of discrete illite in the Patala shale, suggests that hydrocarbon might have potentially migrated from the source to the reservoir rock during smectite illitization.

Smectite illitization, geothermometry, R3 zone, Patala Formation, Upper Indus Basin

INTRODUCTION

Organic-rich sediments convert into kerogen at ca. 50 °C, subsequently changing into crude oil between 50 and 100 °C. Meanwhile, smectite starts diagenetic transformation into illite through inter-stratified illite-smectite (I-Sm) between 50 and 100 °C (Ali et al., 2021; Best, 2013). Smectite adsorbs the crude oil, forms organo-clay complexes, and catalyzes kerogen conversion into liquid hydrocarbon (Jiang, 2012; Li et al., 2017). Smectite illitization induces high pore fluid pressure, which causes dehydration of smectite containing 40 vol.% water. This forcible dehydration prompts the hydrocarbon migration from the source to a reservoir rock (Jiang, 2012; Li et al., 2017; Ali et al., 2021).

✉e-mail: asghar.ali@uop.edu.pk

Reichweite (R) categorizes various types of interstratification in I-Sm, including disordered R0, short-range ordered R1, and long-range ordered R3, which coincide with immature, mature, and mature to postmature hydrocarbon generation zones, respectively (Reynolds, 1980; Pollastro, 1993; Jiang, 2012; Ali et al., 2021). The R1 to R3 conversion at ca. 175–180 °C indicates the upper limit of the oil generation zone, with subsequent methane generation occurring in the overmature R3 zone (Pollastro, 1993). Therefore, the simultaneous transformation of random to ordered I-Sm and hydrocarbon generation establish smectite illitization as a reliable tool for assessing the thermal maturity of hydrocarbon source rocks (Scotchman, 1987; Velde and Espitalié, 1989; Jiang, 2012; Jozanikohan et al., 2016; Ola et al., 2018; Green et al., 2020).

The current research focuses on smectite illitization-based hydrocarbon generation potential and thermal maturity of the Patala Formation exposed in Tirah, NW Pakistan. The Patala Formation has been proven as a primary hydrocarbon source rock in the Upper Indus Basin, except for the Dhurnal field (Fazeelat et al., 2010). The hydrocarbon generation potential and thermal maturity of the Patala Formation have not been previously studied in Tirah. Similarly, smectite illitization is being utilized as a geothermometer for hydrocarbon source rocks in the Upper Indus Basin for the first time. Smectite illitization of the Patala Formation is calculated using X-ray diffraction (XRD) and scanning electron microscopy with energy-dispersive X-ray (SEM-EDX). Additionally, the total organic content of the Patala shale is determined through a total organic carbon (TOC) analysis.

REGIONAL GEOLOGY

Tectonic setting. The Tirah Range lies northwest of the Upper Indus Basin. The NE–SW-oriented Indus Basin is the largest hydrocarbon-generating sedimentary basin of Pakistan that covers an area of ca. 54 000 km^2 (Sheikh and Giao, 2017). The Precambrian basement rocks divide this giant basin into the Upper, Middle, and Lower Indus basins (Fig. 1) (Miraj et al., 2021). The Middle Indus Basin is separated from the Upper and Lower Indus basins by the Sargodha and Jackobabad highs, respectively (Miraj et al., 2021). The Indus River divides the Upper Indus Basin into the Kohat and Potwar subbasins (Afzal et al., 2009).

The late Paleocene to early Eocene Patala Formation is the last remnant of marine deposition in the northwestern Upper Indus Basin. The absence of middle to late Eocene rocks from the northwestern Upper Indus Basin marks the early closure of the Tethys seaway in the early Eocene (Wadood et al., 2021). Meanwhile, the Tethys seaway was open in the eastern, central, and western parts of the Upper Indus Basin. Complete closure of the Tethys seaway occurred in the middle Eocene as a result of the collision of the Indian Plate with the southern amalgamated parts of the Eurasian Plate (Wadood et al., 2021). Consequently, the synorogenic-sediment influx to the Upper Indus Basin started in the early Miocene (Pivnik and Wells, 1996), which resulted in the direct deposition of the Murree Formation over the Patala Formation.

Stratigraphy. The exposed stratigraphic units in the study area include the Jurassic Samana Suk Formation, the Paleocene Hangu Formation and Lockhart Limestone, the late Paleocene to early Eocene Patala Formation, and the Miocene Murree Formation (Figs. 1, 2). The Paleocene and younger rocks show an overturned contact in the study area. Additionally, the Jurassic Samana Suk Formation thrusts over the Miocene Murree Formation along the Sra Wela Thrust (Fig. 1).

The Patala Formation comprises alternate beds of shale and limestone in Tirah (Fig. 3*c*, *d*). The shale is light gray to black, and the limestone is white to light grayish. The limestone consists of larger benthic foraminifera (LBF; Lockhartia, Assilina, Nummulites, and Miscellanea), smaller benthic foraminifera (SBF; Miliolids), ostracods, and fossil fragments (Fig. 4) (Hanif et al., 2013). The Patala Formation is ca. 70 m thick in the studied section (Fig. 2).

MATERIALS AND METHODS

Materials. A total of six shale samples from the Patala Formation were selected for XRD. Four of these samples were also analyzed for SEM-EDX and TOC. Shale samples for XRD and EDX were washed and dried. The dried samples were crushed and powdered with an agate mortar. The powdered samples were treated with the acetic acid–sodium acetate buffer solution for the dissolution of carbonates. Moreover, the samples were treated with hydrogen peroxide for the removal of organic content. Following chemical treatment, samples were disintegrated through sonication. The disintegrated clay samples were separated into different fractions through centrifugation, and the finest clay fraction was collected for further analysis (Środoń, 2006; Środoń et al., 2009).

Methods. XRD analysis. Mineral phases in the clay fraction of the Patala shale were detected using XRD in the Centralized Resource Laboratory, University of Peshawar. Samples were scanned by XRD in AD as well as EG-solvated forms. Clay slides were heated at 60 °C overnight in a desiccator filled to a depth of 1 cm with EG (Patarachao et al., 2018). The samples were analyzed using a JDX-3532 (JEOL-Japanese) *X*-ray diffractometer with CuKα radiation at 40 kV and 30 mA. A scattering slit of 2 mm along with divergent and

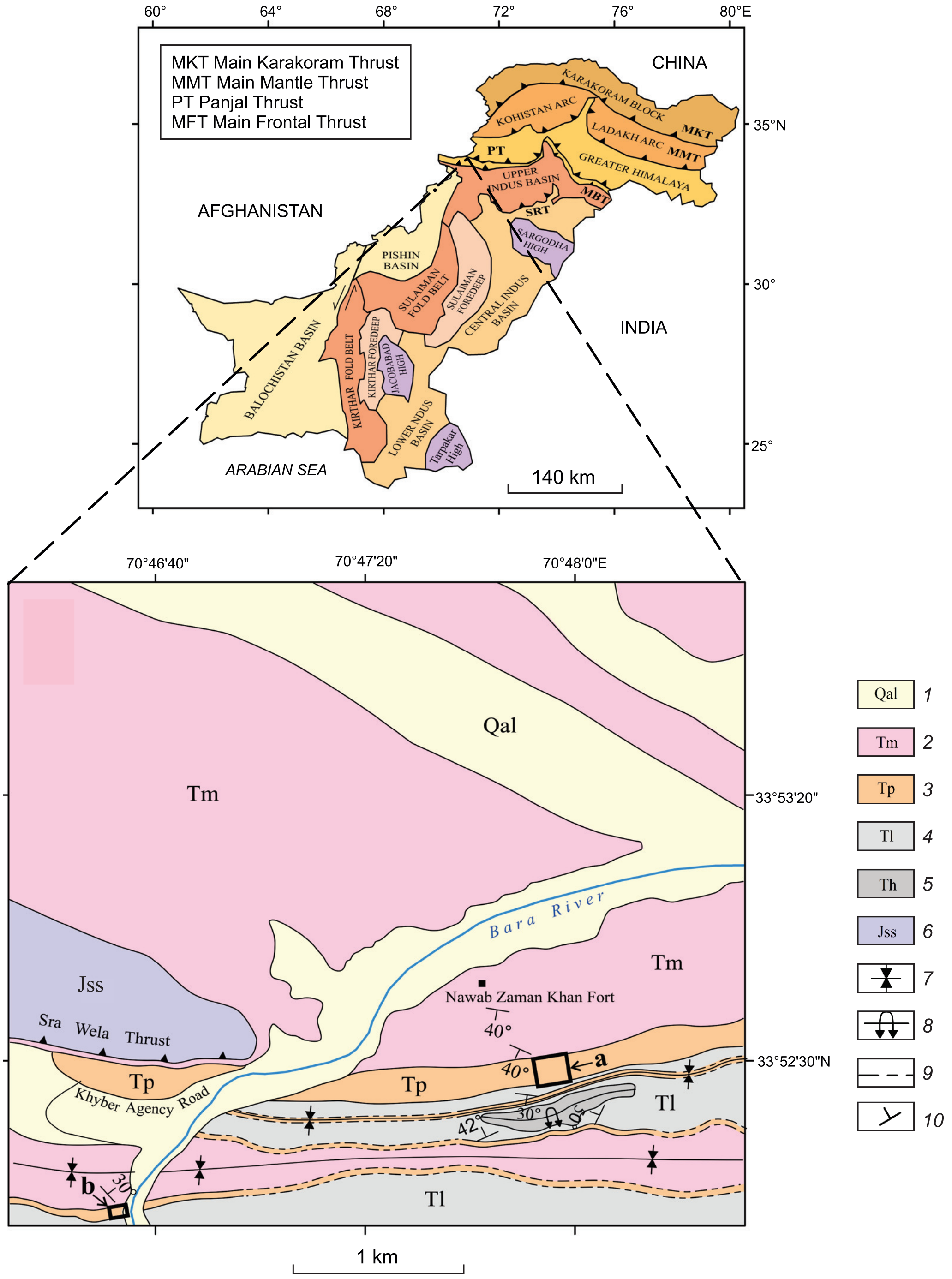

Fig. 1. Inset map of Pakistan showing the distribution of different tectonic units (Kazmi and Jan, 1997).

Geological map showing the major lithologic units and structural architecture of the study area, measured section, and location of TS 01–TS 05 (*a*) and TS 06 (*b*). *1* – alluvium, *2* – Murree Formation, *3* – Patala Formation, *4* – Lockhart Formation, *5* – Hangu Formation, *6* – Samana Suk Formation, *7* – syncline, *8* – overturned anticline, *9* – inferred contact, *10* – strike and dip of bedding.

---

receiving slits of 1° were used. The samples were scanned in 0–35° 2θ range with a single-second step time and an angle of 0.050°.

SEM-EDX analysis. Morphological examination of the Patala shale was performed using an SEM-JSM5910 scanning electron imaging detector with maximum magnification power of 300,000x and a maximum resolution of 2.3 nm. Gold-coated sample chips were mounted on aluminum stubs, and photomicrographs were taken at resolution scales of 8, 10, 20, and 40 µm. Chemical analysis of the treated clay fraction was performed using EDX-INCA200 attached to SEM-JSM5910.

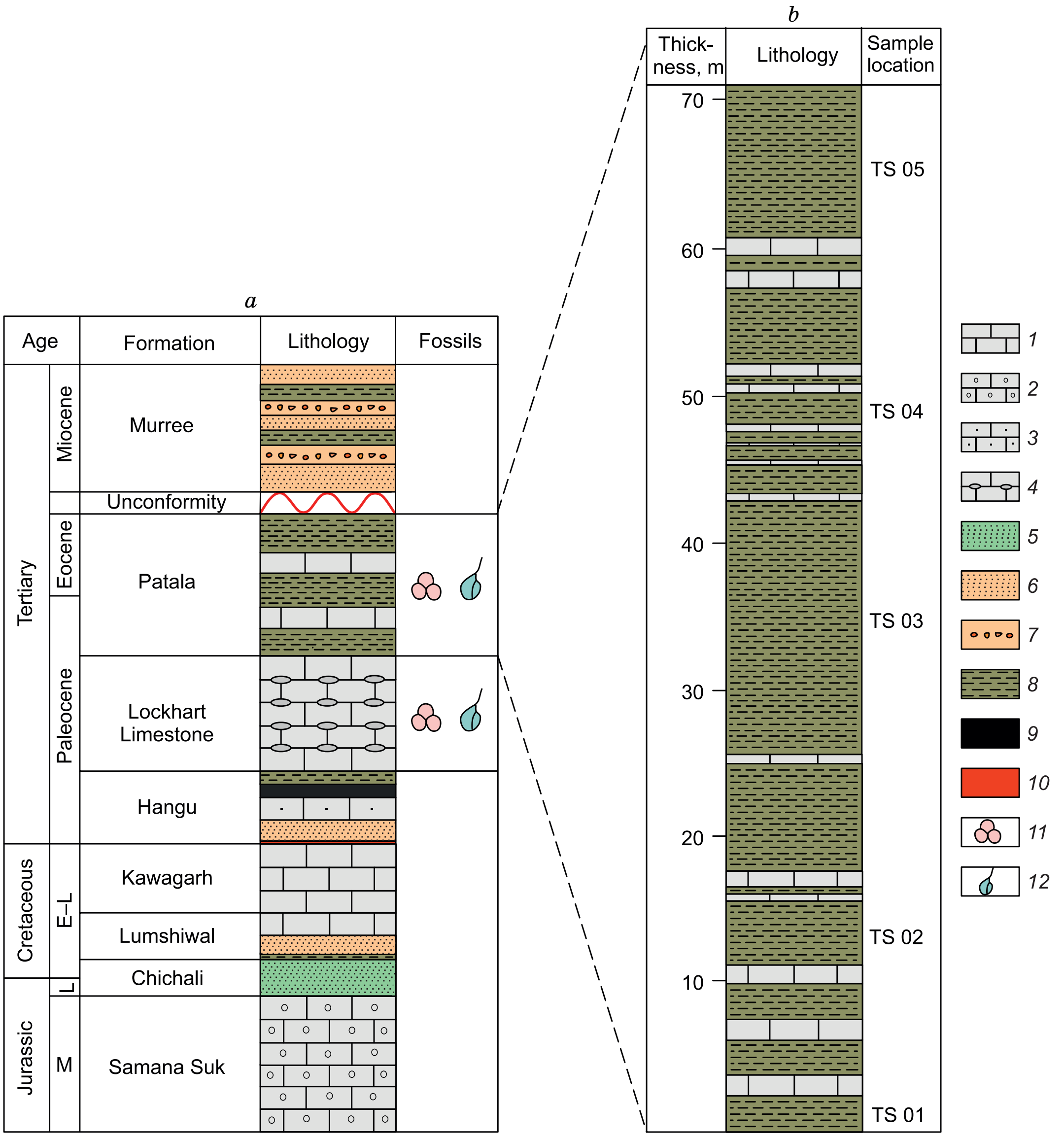

Fig. 2. ***a*** **– Generalized stratigraphic column showing the Jurassic to Miocene stratigraphy of Tirah. The middle to late Eocene and Oligocene stratigraphic units of the Upper Indus Basin are missing, which is marked as unconformity (modified after Khan et al., 2018, 2022). E – early, M – middle, L – late. The Cretaceous units are exposed outside of the map (Fig. 1).** ***b*** **– Detailed stratigraphic log of the Patala Formation exposed in Tirah.**

1 – limestone, *2* – oolitic Limestone, *3* – sandy limestone, *4* – nodular limestone, *5* – glauconitic sandstone, *6* – sandstone, *7* – conglomerate, *8* – shale, *9* – coal, *10* – bauxite and laterite, *11* – foraminifera, *12* – fossil fragments.

TOC. The TOC of the Patala shale was evaluated at the Hydrocarbon Development Institute of Pakistan. Samples weighing 100 to 150 mg were washed and dried overnight in an oven at 40°C. The dried samples were crushed, ground, and powdered. The powdered samples were treated with 5% HCl to remove inorganic carbon. The samples were dried on a hotplate at 40 °C and subjected to further evaluation using Leuco CS-300. Carbon content was determined by Infrared detectors in the TOC analyzer.

RESULTS

XRD analysis. Mineral phases. Illite, quartz, chlorite, kaolinite, muscovite, and calcite are detected in the Patala clay fraction (Fig. 5). Discrete illite phases are detected with reflections of 001, 002, 003, and $13\bar{1}$ planes. Illite 001 is identified at 9.9 Å in TS 02, TS 04, TS 05, and TS 06, whereas in TS 01 and TS 03 it is detected at 10.3 Å (Fig. 5). Reflection of illite 002 is detected at 5.01 Å in TS 04, TS 05, and TS 06. Diffraction peaks from illite 003 and illite 13$\overline{1}$ are detected at 3.34 Å and 2.56 Å, respectively (Fig. 5). Quartz 100 is identified at 4.26 Å in TS 01, TS 02, TS 03, TS 05, and TS 06, whereas quartz 101 is detected at 3.34 Å. Illite 003 and quartz 101 reflections overlap and result in a high-intensity peak at 3.34 Å (Fig. 5). Furthermore, chlorite 002 is detected at 7.05 Å, and chlorite 004 is identified at 3.52 Å in TS 01, TS 03, TS 04, and TS 05 (Fig. 5). Kaolinite 001 in TS 01-05 and kaolinite 002 in TS 01, TS 03, TS 04, and TS 05 are identified at 7.06 Å and 3.53 Å, respectively. Reflection of muscovite 11$\overline{1}$ is detected at 4.45 Å in TS 02 and TS 04, whereas muscovite 025 is detected at 2.90 Å in TS 02 (Fig. 5). Moreover, the diffraction peak of calcite 104 is detected at 3.03 Å in TS 06 (Fig. 5*f*).

Polymorphism in illite and muscovite. Discrete illite phases are detected with 1M, $2M_1$, and $2M_2$ polymorphs. Illite 002 and illite 003 are identified as 1M, whereas illite 13$\overline{1}$ and illite 001 are determined as $2M_1$ and $2M_2$. Similarly, the diffraction peaks of muscovite 11$\overline{1}$ and muscovite 025 are identified as $2M_1$ (Fig. 5).

SEM-EDX analysis. Chemistry of the clay fraction. The Patala clay fraction geochemically consists of SiO_2, Al_2O_3, Fe_2O_3, K_2O, MgO, CaO, TiO_2, SO_2, and C (Table 1). The percentage of SiO_2 varies from 56.78 to 60.85% in TS 01, TS 03, and TS 05 but is 32.24% in TS 06. The share of Al_2O_3 varies from 12.15 to 19.34%, while that of Fe_2O_3 ranges from 11.58 to 12.22%. The share of K_2O fluctuates between 4.40 and 6.97% in TS 01, TS 03, and TS 05 but is 2.18% in TS 06. The percentage of MgO varies from 2.10 to 2.36%. The percentage of CaO varies from 0.85 to 2.28% in TS 01, TS 03, and TS 05 but is 21.76% in TS 06. The abundance of TiO_2 ranges from 1.01 to 2.03%. Moreover, TS 06 is detected with 1.79% SO_2 and 15.02% C (Table 1).

Morphology of illite. The authigenic origin of illite was confirmed using SEM. In situ growth of pure illite with characteristic platy habit and curly edges is observed in the Patala shale (Fig. 6). Simultaneous EDX analysis of the same samples reveals a considerable amount of SiO_2, Al_2O_3, and Fe_2O_3. The percentage of K_2O is relatively higher than that of CaO, MgO, and TiO_2 in TS 01, TS 03, and TS 05 (Fig. 6*a–c*). However, TS 06 is detected with relatively high percentage of TiO_2 and CaO as compared with K_2O and MgO (Fig. 6*d*).

TOC of the Patala Formation. The Patala shale yielded low to high TOC, including 0% TOC from TS 01 and TS 03, 0.1% TOC from TS 05, and 1.2% TOC from TS 06 (Fig 1; Table 2). The hydrocarbon generation potential of TS 01, TS 03, and TS 05 is low, whereas that of TS 06 is high (Table 2).

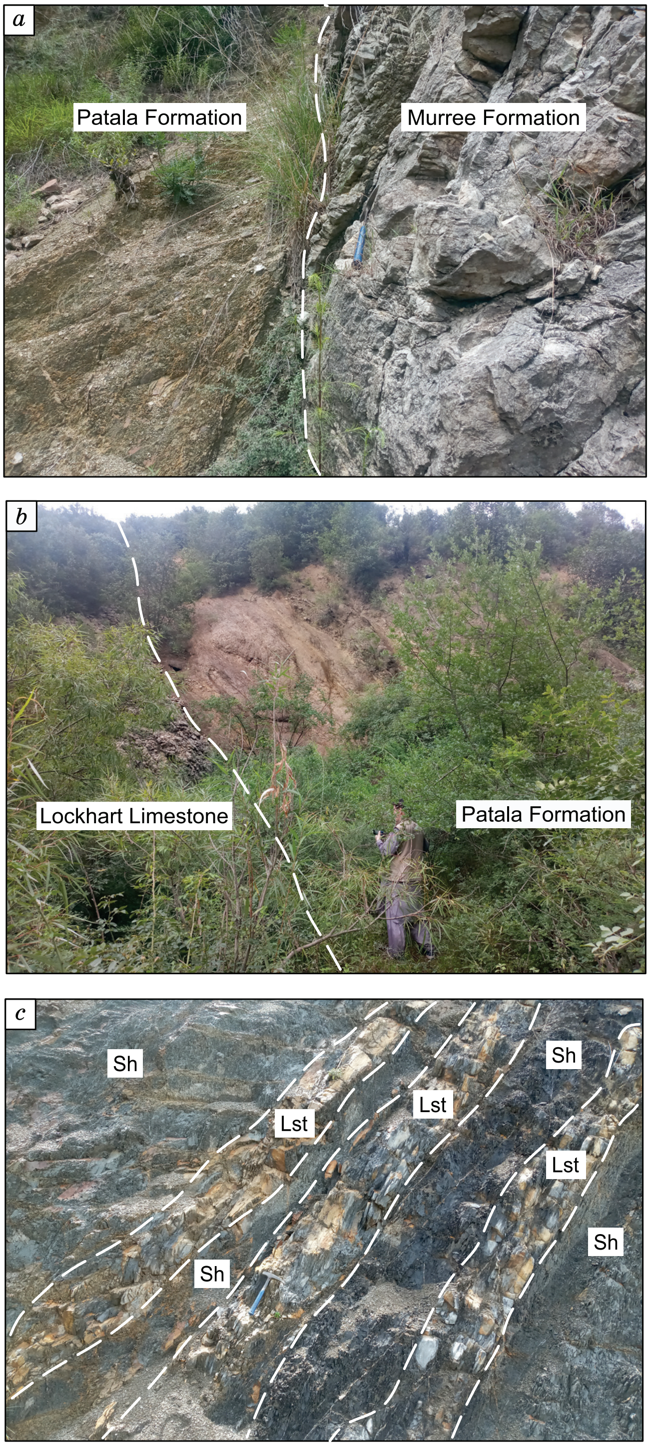

Fig. 3. Photographs showing:

a – the upper overturned contact between the Patala and Murree formations, *b* – the lower overturned contact between the Lockhart Limestone and the Patala Formation, *c* – Patala interbedded shale and limestone. Sh – shale, Lst – limestone.

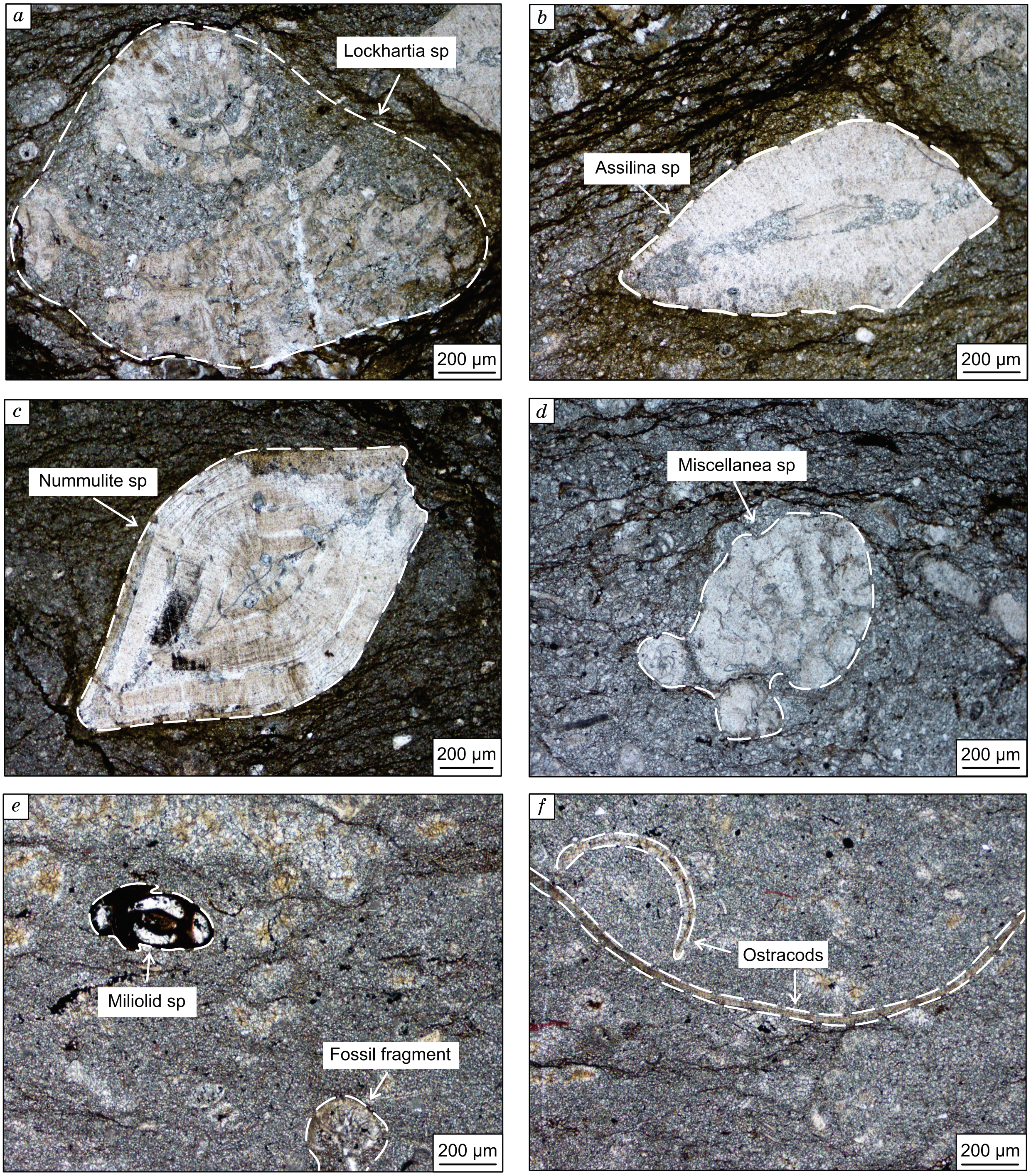

Fig. 4. Photomicrographs of: *a* – LBF Lockhartia, *b* – LBF Assilina, *c* – LBF Nummulite, *d* – LBF Miscellanea sp., *e* – SBF Miliolidsp, *f* – Ostracods.

DISCUSSION

The extent of smectite illitization in the Patala Formation. Discrete smectite appears at or above 15 and 17 Å in AD and EG-solvated XRD patterns, respectively (McIntosh et al., 2021). The AD patterns of the Patala shale are not detected with any peak at or above 15 Å (Fig. 5). Similarly, no peak is observed at or above 17 Å in the EG-solvated patterns of the Patala shale (Fig. 5), which suggests the absence of discrete smectite. According to Pataracha o et al. (2018), the presence of I-Sm results in a broad and asymmetric peak at the lower angle side of illite 001 in AD patterns. The peak becomes sharper and symmetric upon glycolation. Also,

Table 1. **Percentage of major oxides in the Patala clay fraction**

Major oxides	TS 01	TS 03	TS 05	TS 06
SiO_2	59.18	56.78	60.85	32.24
Al_2O_3	17.78	19.34	16.9	12.15
Fe_2O_3	12.22	12.10	11.58	11.62
K_2O	4.40	6.97	5.62	2.18
MgO	2.36	2.10	2.17	2.23
CaO	2.28	0.95	0.85	21.76
TiO_2	1.78	1.76	2.03	1.01
SO_2	—	—	—	1.79
C	—	—	—	15.02
Total	100	100	100	100

Table 2. **Percentage of TOC and hydrocarbon generation potential of the Patala shale in Tirah**

Sample no.	TOC, %	Hydrocarbon potential
TS 01	0.0	Low
TS 03	0.0	Low
TS 05	0.1	Low
TS 06	1.2	High

new I-Sm peaks may appear at the higher angle side of the illite 001 peak in EG-solvated pattern (Patarachao et al., 2018). Comparison between the AD and EG-solvated patterns of the Patala shale reveals the absence of I-Sm in detectable quantities, because no distinction is observed between the AD and EG-solvated XRD patterns (Fig. 5). However, discrete illite is detected in both the AD and the EG-solvated XRD patterns of the Patala shale (Fig. 5). The absence of discrete smectite along with I-Sm and the presence of illite in the Patala shale indicate that the Patala Formation has entered into the R3 illitization zone of Pollastro (1993) (Fig. 7).

Polymorphic transformation of illite. Polymorphic transformation of illite from $1M_d$ to $2M_1$ occurs during smectite illitization (Merriman, 2006; Chen and Wang, 2007; Bozkaya et al., 2012; Galán and Ferrell,

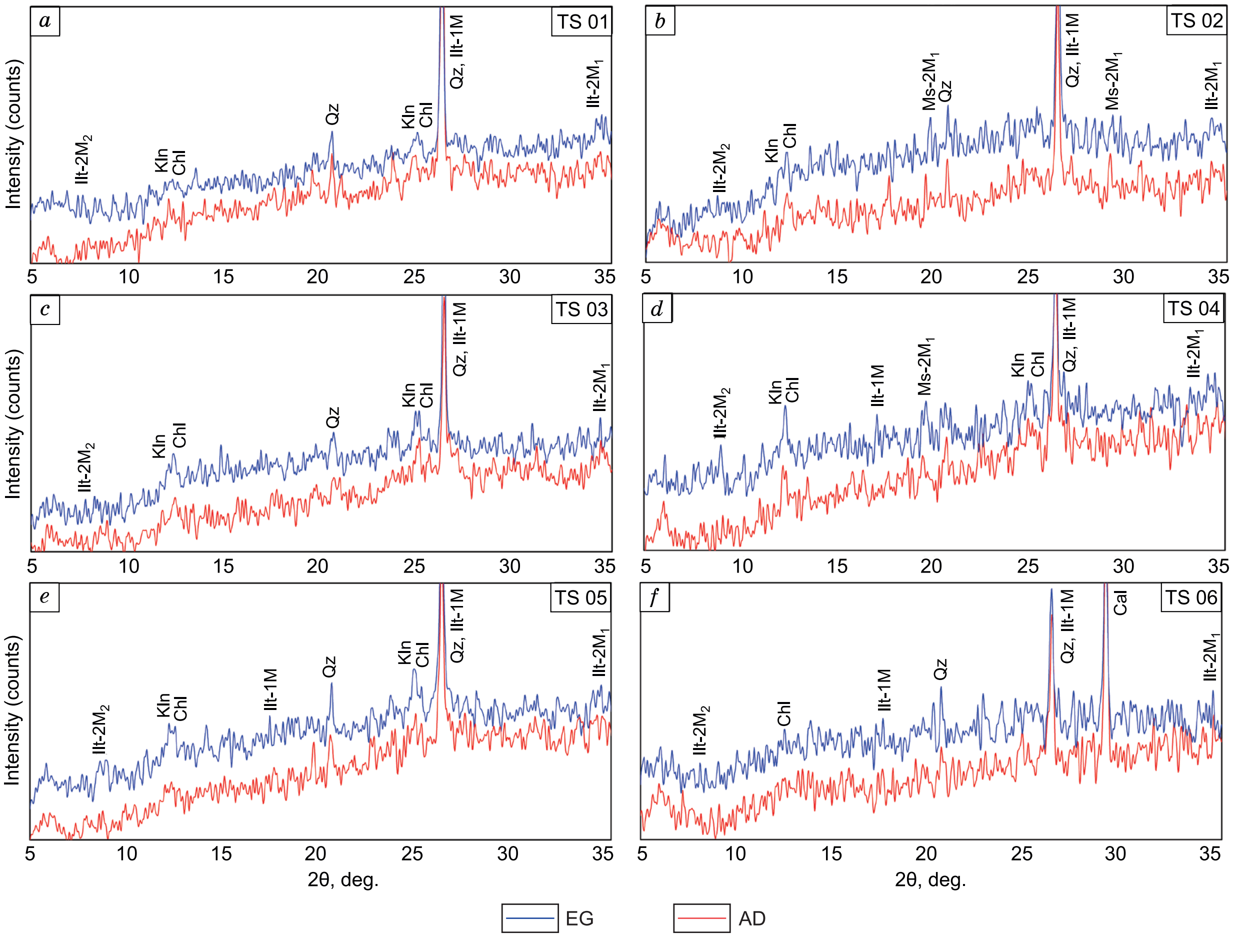

Fig. 5. Air-dried (AD) and ethylene glycol (EG)-solvated XRD patterns of TS 01, TS 02, TS 03, TS 04, TS 05, and TS 06 from the Patala Formation. Comparison between AD and EG-solvated XRD patterns reveals the absence of discrete smectite and I-Sm phases.

Detection of discrete illite indicates that the Patala Formation has entered the R3 illitization zone. Ilt – illite, Kln – kaolinite, Chl – chlorite, Qz – quartz, Ms – muscovite, Cal – calcite (Whitney and Evans, 2010).

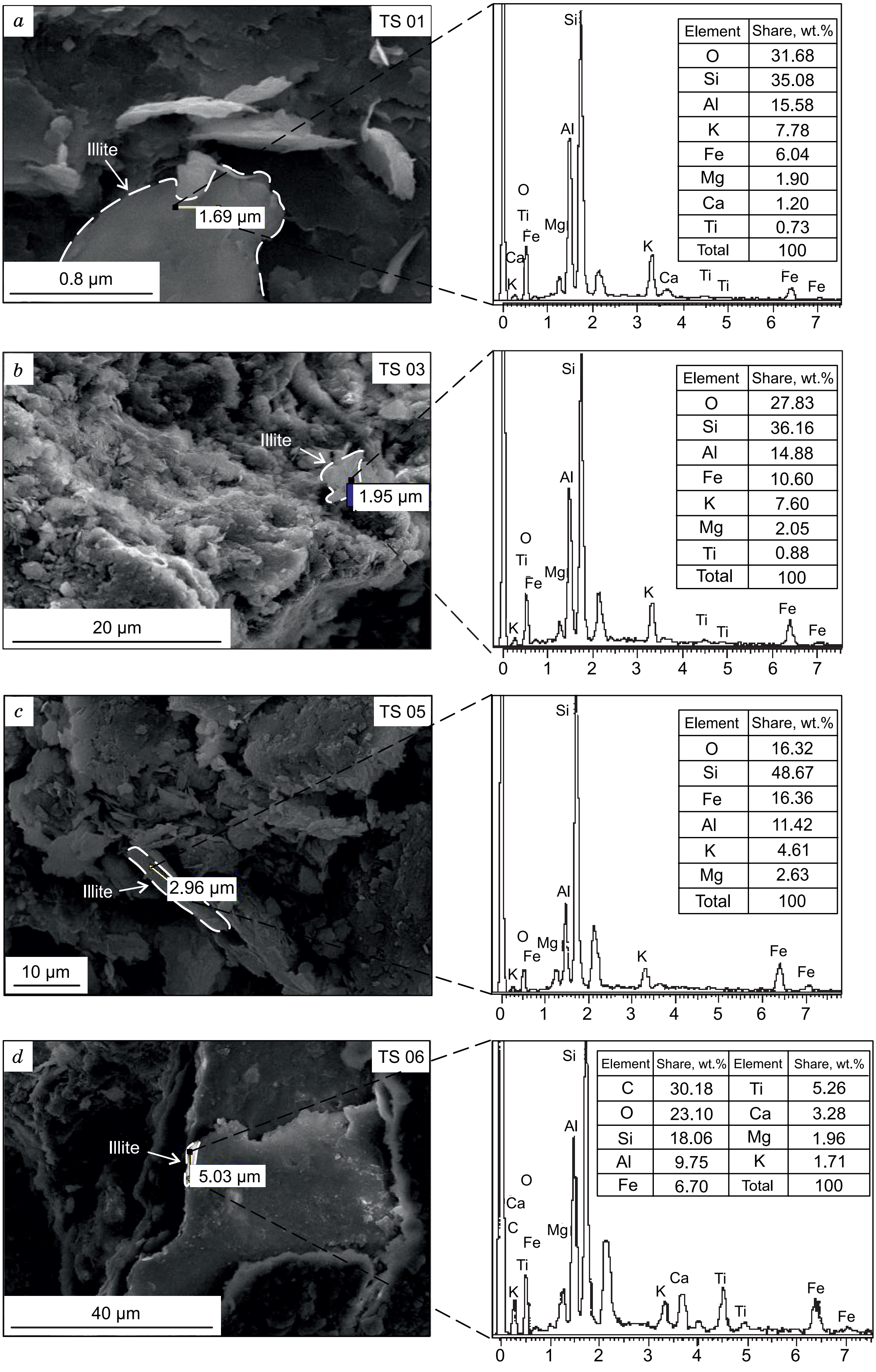

Element	Share, wt.%
O	31.68
Si	35.08
Al	15.58
K	7.78
Fe	6.04
Mg	1.90
Ca	1.20
Ti	0.73
Total	100

Element	Share, wt.%
O	27.83
Si	36.16
Al	14.88
Fe	10.60
K	7.60
Mg	2.05
Ti	0.88
Total	100

Element	Share, wt.%
O	16.32
Si	48.67
Fe	16.36
Al	11.42
K	4.61
Mg	2.63
Total	100

Element	Share, wt.%	Element	Share, wt.%
C	30.18	Ti	5.26
O	23.10	Ca	3.28
Si	18.06	Mg	1.96
Al	9.75	K	1.71
Fe	6.70	Total	100

Fig. 6. SEM images showing in situ growth of platy illite crystals indicating R3 illitization zone.

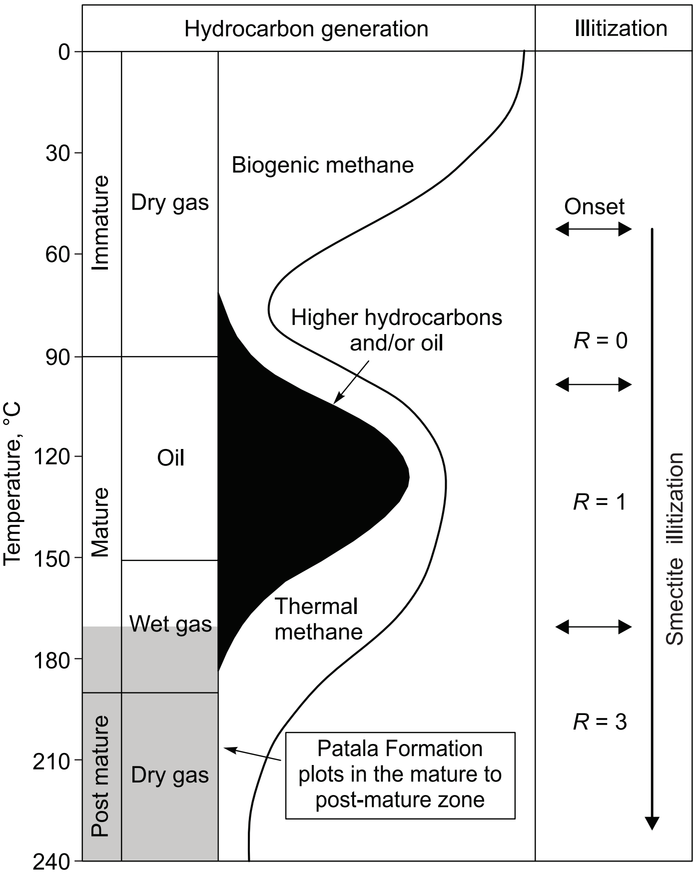

Fig. 7. Temperature-based relationship between hydrocarbon generation and illitization. The maturity zone of the Patala Formation has been constrained in the temperature range of R3, which coincides with the mature to postmature zone of Pollastro (1993).

2013; Wang et al., 2016; Hu et al., 2018; Süssenberger et al., 2018; Gorokhov et al., 2019; Nguyen-Thanh et al., 2021). The conversion process starts during late diagenesis in the low anchizone and terminates in the high anchizone (Merriman, 2006; Galán and Ferrell, 2013; Hu et al., 2018). Therefore, the polymorphic transformation of illite is a useful indicator of diagenetic evolution into the anchizone, where the anchizone corresponds to a temperature between 200 and 300 °C (Wang et al., 2004, 2016; Merriman, 2006; Galán and Ferrell, 2013; Hu et al., 2018). Additionally, muscovite polymorphs are identical to illite in petrogenetic character (Wang et al., 2003; Merriman, 2006; Galán and Ferrell, 2013). The detection of illite and muscovite peaks with 2M$_1$ polymorph in the Patala shale indicates that the Patala Formation has entered the late-stage diagenetic zone or the anchizone (Fig. 5). The temperature range of the late diagenesis or the anchizone lies in the R3 illitization zone (Fig. 7).

Cation exchange during smectite illitization. Smectite illitization occurs as a result of the addition of K^+ to the interlayer space of smectite. Meanwhile, the expulsion of Ca^{2+}, Na^+, and Mg^{2+} from the smectite interlayers occurs (Cai et al., 2018; Morad et al., 2000; McIntosh et al., 2021). In addition, tetrahedral Al^{3+} replaces Si^{4+}, which causes an increased Al/Si ratio in illite as compared with smectite (Pollastro, 1985; McIntosh et al., 2021). The relatively high percentage of K_2O to CaO in TS 01, TS 03, and TS 05 and MgO in TS 03 and TS 05 illustrates the exchange of K^+ with Ca^{2+} and Mg^{2+} in the smectite interlayers during illitization (Table 1). However, the relatively high percentage of CaO in TS 06 indicates calcium carbonate, which is also detected in the XRD pattern of the same sample (Table 1); (Fig. 5*f*). Moreover, the abundance of Al_2O_3 demonstrates that Al^{3+} was available in considerable amounts for the substitution of Si^{4+}, which led to illitization in the Patala Formation (Table 1).

Authigenic illite crystals. Patala shale reveals in situ growth of pure illite with platy habit and curly edges (Fig. 6). Illite in I-Sm initially grows with ribbons and flake-like appearance. The ribbons coalesce upon illitization, which results in the characteristic platy habit of discrete illite (Keller et al., 1986; Ylagan et al., 2000; Meunier and Velde, 2004; Al-Ramadan, 2014; Nguyen-Thanh et al., 2021). The illite habit evolves as a function of the depth of burial. At shallower depths, illite appears as xenomorphic flakes and filaments in the R0 zone (Inoue, 1986; Nguyen-Thanh et al., 2021). Filamentous crystals convert to subhedral laths in the R1 illitization zone. In the R3 zone, illite laths transform into isometric pseudohexagonal or platy crystals (Inoue, 1986; Nguyen-Thanh et al., 2021). Therefore, the platy habit of authigenic illite in the Patala shale indicates the R3 zone (Fig. 6).

A considerable amount of Si and Al and the relatively abundant percentage of K to Ca and Mg confirm the presence of discrete illite in the Patala shale (Fig. 6*a–c*) (Welton, 1984).

Source rock potential of the Patala Formation. The Patala Formation yields 0.5 to 3.5% TOC (on average, 1.4%) in the Upper Indus Basin (Wandrey et al., 2004; Fazeelat et al., 2010). However, the Patala Formation in Tirah yields low to high amounts of TOC, which suggests a poor to good source rock in the region (Table 2). Similarly, the absence of discrete smectite and I-Sm, combined with the presence of discrete illite in the Patala shale, indicates that hydrocarbon might have potentially migrated from the source to the reservoir rock during smectite illitization (Figs. 5–7).

CONCLUSIONS

– Smectite illitization geothermometry is utilized to assess the thermal maturity and hydrocarbon generation potential of the Patala Formation in Tirah. Comparison between AD and EG-solvated patterns reveals the absence of discrete smectite and I-Sm. However, discrete illite phases are consistently detected across all XRD patterns. This suggests that the Patala Formation lies in the R3 illitization zone.

– Detection of illite-2M_1 in the Patala shale demonstrates that the Patala Formation has entered the late-stage diagenetic zone or the anchizone, which lies in the R3 zone of smectite illitization.

– The considerable amount of SiO_2 and Al_2O_3 in the Patala clay fraction indicates the substitution of Si^{4+} by Al^{3+} in smectite. Likewise, the relatively high percentage of K_2O to CaO and MgO illustrates the exchange of K^+ with Ca^{2+} and Mg^{2+} in the smectite interlayers during illitization.

– The TOC of the Patala shale potentially indicates a poor to good source rock. Similarly, the absence of discrete smectite and I-Sm, combined with the presence of discrete illite in the Patala shale, indicates that hydrocarbon might have potentially migrated from the source to the reservoir rock during smectite illitization.

ACKNOWLEDGEMENT

We appreciate the Department of Geology, Centralized Resource Laboratory, National Centre of Excellence in Geology, University of Peshawar, and the Hydrocarbon Development Institute of Pakistan for research facilities.

REFERENCES

Afzal, J., Williams, M., Aldridge, R.J., 2009. Revised stratigraphy of the lower Cenozoic succession of the Greater Indus Basin in Pakistan. J. Micropalaeontol. 28 (1), 7–23, doi: copernicus.org/articles/28/7/2009/.

Ali, A., Salman, M., Ahmad, R., 2021. Smectite illitization of the Talhar shale, Lower Goru Formation, Southern Indus Basin, Pakistan. J. Pet. Explor. Prod. Technol. 11 (6), 2315–2325, doi: 10.1007/s13202-021-01183-5.

Al-Ramadan, K., 2014. Illitization of smectite in sandstones: the Permian Unayzah reservoir, Saudi Arabia. Arab J. Sci. Eng. 39, 407–412, doi: 10.1007/s13369-013-0913-6.

Best, M.G., 2013. Igneous and Metamorphic Petrology. Wiley, Blackwell.

Bozkaya, Ö.,Yalçın, H., Göncüoğlu, M.C., 2012. Diagenetic and very low-grade metamorphic characteristics of the Paleozoic series of the Istanbul Terrane (NW Turkey). Swiss J. Geosci. 105, 183–201, doi: 10.1007/s00015-012-0108-2.

Cai, J., Du, J., Chen, Z., Lei, T., Zhu, X., 2018. Hydrothermal experiments reveal the influence of organic matter on smectite illitization. Clays Clay Miner. 66 (1), 28–42, doi: 10.1346/CCMN.2017.064084.

Chen, T., Wang, H., 2007. Microstructure characteristics of illite from Chuanlingou Formation of Changcheng System in Jixian County, Tianjin City. Sci. China, Ser. D Earth Sci. 50 (10), 1452–1458, doi: 10.1007/s11430-007-0090-0.

Fazeelat, T., Jalees, M.I., Bianchi, T.S., 2010. Source rock potential of Eocene, Paleocene and Jurassic deposits in the subsurface of the Potwar Basin, northern Pakistan. J. Pet. Geol. 33 (1), 87–96, doi: 10.1111/j.1747-5457.2010.00465.x.

Galán, E., Ferrell, R.E., 2013. Genesis of clay minerals, in: Handbook of Clay Science. Developments in Clay Science 5, pp. 83–126, doi: 10.1016/B978-0-08-098258-8.00003-1.

Green, H., Šegvić, B., Zanoni, G., Omodeo-Salé, S., Adatte, T., 2020. Evaluation of shale source rocks and clay mineral diagenesis in the Permian Basin, USA: Inferences on basin thermal maturity and source rock potential. Geosciences 10 (10), 381, doi: 10.3390/geosciences10100381.

Gorokhov, I.M., Zaitseva, T.S., Kuznetsov, A.B., Ovchinnikova, G.V., Arakelyants, M.M., Kovach, V.P., Konstantinova, G.V., Turchenko, T.L., Vasil'eva, I.M., 2019. Isotope systematics and age of authigenic minerals in shales of the Upper Riphean Inzer Formation, South Urals. Stratigr. Geol. Correl. 27, 133–158, doi: 10.1134/S0869593819020035.

Hanif, M., Ali, F., Afridi, B.Z., 2013. Depositional environment of the Patala Formation in biostratigraphic and sequence stratigraphic context from Kali Dilli Section, Kala Chitta Range, Pakistan. J. Himal. Earth Sci. 46 (1), 55–65.

Hu, D., Zhan, N., Zhang, J., Li, Y., Sun, G., 2018. Diagenesis and very low-grade metamorphism of the Upper Permian Yangjiagou Formation in eastern Changchun, China: Evidence from clay mineral geothermobarometers. Acta Geol. Sin. 92 (3), 1053–1062, doi: 10.1111/1755-6724.13591.

Inoue, A., 1986. Morphological change in a continuous smectite-to-illite conversion series by scanning and transmission electron microscopies. J. Coll. Arts Sci., Chiba Univ. B-19, 23–33.

Jiang, S., 2012. Clay minerals from the perspective of oil and gas exploration, in: Clay Minerals in Nature – Their Characterization, Modification and Application. IntechOpen, Rijeka, pp. 21–38, doi: 10.5772/47790.

Jozanikohan, G., Sahabi, F., Norouzi, G.H., Memarian, H., Moshiri, B., 2016. Quantitative analysis of the clay minerals in the Shurijeh Reservoir Formation using combined X-ray analytical techniques. Russ. Geol. Geophys. 57 (7), 1048–1063, doi: 10.1016/j.rgg.2016.06.005.

Kazmi, A.H., Jan, M.Q., 1997. Geology and Tectonics of Pakistan. Graphic Publishers, Karachi.

Keller, W., Reynolds, R., Inoue, A., 1986. Morphology of clay minerals in the smectite-to-illite conversion series by scanning electron microscopy. Clays Clay Miner. 34, 187–197, doi: 10.1346/CCMN.1986.0340209.

Khan, N., Anjum, N., Ahmad, M., Awais, M., Ullah, N., 2018. Hydrocarbon source rock potential evaluation of the Late Paleocene Patala Formation, Salt Range, Pakistan: Organic geochemical and palynofacies approach. J. Earth Syst. Sci. 127 (7), 98, doi: 10.1007/s12040-018-0998-0.

Khan, N., Ullah, W., Siyar, S.M., Wadood, B., Ayyub, T., Ullah, T., 2022. Hydrocarbon source rock assessment of the shale and coal bearing horizons of the Early Paleocene Hangu Formation in Kala-Chitta Range, Northwest Pakistan. J. Pet. Explor. Prod. Technol. 12 (8), 2155–2172, doi: 10.1007/s13202-021-01433-6.

Li, Y., Cai, J., Wang, X., Hao, Y., Liu, Q., 2017. Smectite-illitization difference of source rocks developed in saline and fresh water environments and its influence on hydrocarbon generation: A study from the Shahejie Formation, Dongying Depression, China. Mar. Pet. Geol. 80, 349–357, doi: 10.1016/j.marpetgeo.2016.12.004.

McIntosh, J.A., Tabor, N.J., Rosenau, N.A., 2021. Mixed-layer illite-smectite in Pennsylvanian-aged paleosols: Assessing sources of illitization in the Illinois Basin. Minerals 11 (2), 108, doi: 10.3390/min11020108.

Merriman, R.J., 2006. Clay mineral assemblages in British Lower Palaeozoic mudrocks. Clay Miner. 41 (1), 473–512, doi: 10.1180/0009855064110204.

Meunier, A., Velde, B., 2004. Illite: Origins, Evolution and Metamorphism. Springer, Berlin, Heidelberg.

Miraj, M.A.F., Ali, A., Javaid, H., Rathore, P.W.S., Ahsan, N., Saleem, R.F., Afgan, S. Malik, M.B., 2021. An integrated approach to evaluate the hydrocarbon potential of Jurassic Samana Suk Formation in Middle Indus Basin, Pakistan. Kuwait J. Sci. 48 (4), doi: 10.48129/kjs.v48i4.9193.

Morad, S., Ketzer, J.M., De Ros, L.F., 2000. Spatial and temporal distribution of diagenetic alterations in siliciclastic rocks: implications for mass transfer in sedimentary basins. Sedimentology 47, 95–120, doi: 10.1046/j.1365-3091.2000.00007.x.

Nguyen-Thanh, L., Mählmann, R.F., Hoang-Minh, T., Petschick, R., Reischmann, T., Nesbor, H.D., Fritsche, J.G., 2021. Clay mineral formation in Permian rocks of a geothermal borehole at Northern Upper Rhine Graben, Germany. Int. J. Earth Sci. 110, 1415–1438.

Ola, P.S., Aidi, A.K., Bankole, O.M., 2018. Clay mineral diagenesis and source rock assessment in the Bornu Basin, Nigeria: Implications for thermal maturity and source rock potential. Mar. Pet. Geol. 89, 653–664, doi: 10.1016/j.marpetgeo.2017.10.031.

Patarachao, B., Tyo, D., Zborowski, A., Kung, J., Ng, S., Mercier, P., 2018. XRD Analysis of illite-smectite interstratification in clays from oil sands ores. Adv. X-Ray Anal. 62, 22–31.

Pivnik, D.A., Wells, N.A., 1996. The transition from Tethys to the Himalaya as recorded in northwest Pakistan. Geol. Soc. Am. Bull. 108 (10), 1295–1313, doi: 10.1130/0016-7606(1996)108<1295:TTFTTT>2.3.CO;2.

Pollastro, R.M., 1985. Mineralogical and morphological evidence for the formation of illite at the expense of illite/smectite. Clays Clay Miner. 33, 265–274, doi: 10.1346/CCMN.1985.0330401.

Pollastro, R.M., 1993. Considerations and applications of the illite/smectite geothermometer in hydrocarbon-bearing rocks of Miocene to Mississippian age. Clays Clay Miner. 41, 119–133, doi: 10.1346/CCMN.1993.0410202.

Reynolds, R.C., 1980. Interstratified clay minerals, in: Brindley, G.W., Brown, G. (Eds.), Crystal Structures of Clay Minerals and Their X-Ray Identiftcation. Mineralogical Society, London, pp. 249–303, doi: 10.1180/mono-5.

Scotchman, I.C., 1987. Clay diagenesis in the Kimmeridge Clay Formation, onshore UK, and its relation to organic maturation. Mineral. Mag. 51 (62), 535–551, doi: 10.1180/minmag.1987.051.362.08.

Sheikh, N., Giao, P.H., 2017. Evaluation of shale gas potential in the Lower Cretaceous Sembar Formation, the Southern Indus Basin, Pakistan. J. Nat. Gas Sci. Eng. 44, 162–176, doi: 10.1016/j.jngse.2017.04.014.

Środoń, J., 2006. Identification and quantitative analysis of clay minerals, in: Developments in Clay Science. Elsevier, Amsterdam, Vol. 5, pp. 765–787, doi: 10.1016/S1572-4352(05)01028-7.

Środoń, J., Clauer, N., Huff, W., Dudek, T., Banaś, M., 2009. K–Ar dating of the Lower Palaeozoic K-bentonites from the Baltic Basin and the Baltic Shield: implications for the role of temperature and time in the illitization of smectite. Clay Miner. 44 (3), 361–387.

Süssenberger, A., Schmidt, S.T., Wemmer, K., Baumgartner, L.P., Grobéty, B., 2018. Timing and thermal evolution of fold-and-thrust belt formation in the Ultima Esperanza District, 51°S Chile: Constraints from K–Ar dating and illite characterization. Geol. Soc. Am. Bull., 130 (5–6), 975–998, doi: 10.1130/B31766.1.

Velde, B., Espitalié, J., 1989. Comparison of kerogen maturation and illite/smectite composition in diagenesis. J. Pet. Geol. 12 (1), 103–110, doi: 10.1111/j.1747-5457.1989.tb00223.x.

Wadood, B., Khan, S., Khan, A., Khan, M.W., Liu, Y., Li, H., Ahmad, S., Khan, A., 2021. Diachroneity in the closure of the eastern Tethys Seaway: evidence from the cessation of marine sedimentation in northern Pakistan. Aust. J. Earth Sci. 68 (3), 410–420, doi: 10.1080/08120099.2020.1782472.

Wandrey, C.J., Law, B., Shah, H.A., 2004. Patala-Nammal Composite Total Petroleum System, Kohat-Potwar Geologic Province, Pakistan. US Geological Survey Publication, Bull. 2208-B, doi: 10.3133/b2208B.

Wang, H., Zhou, J., Xu, Q., Liu, C., Zhu, M., 2003. Very low-grade metamorphism of the Meso-Neoproterozoic and the Lower Paleozoic along the profile from Huangtudian to Xianxi in the central-northern part of Hunan Province, China. Sci. China Earth Sci. 46, 672–682, doi: 10.1360/03yd9059.

Wang, H., Chen, T., Wang, H., Zhang, Z., 2004. Anchimetamorphism of the Neoproterozoic and the Lower Paleozoic along the profile of Yuanguping in Western Hunan Province, China. Acta Geol. Sin. 78 (1), 170–176, doi: 10.1111/j.1755-6724.2004.tb00689.x.

Wang, H., Yuan, L., Wang, L., Zhou, Z., An, J., 2016. Very low-grade metamorphism of clastic rocks from the Meso-Neoproterozoic and the Paleozoic along the profile Yueyang-Linxiang in northeastern Hunan Province and its geological implications. Acta Geol. Sin. 90 (5), 1743–1753, doi: 10.1111/1755-6724.12813.

Welton, J.E., 1984. SEM Petrology Atlas. American Association of Petroleum Geologists, Tulsa, Oklahoma, pp. 47–55, doi: 10.1306/Mth4442.

Whitney, D.L., Evans, B.W., 2010. Abbreviations for names of rock-forming minerals. Am. Mineral. 95 (1), 185–187, doi: 10.2138/am.2010.3371.

Ylagan, R.F., Altaner, S.P., Pozzuoli, A., 2000. Reaction mechanisms of smectite illitization associated with hydrothermal alteration from Ponza Island, Italy. Clays Clay Miner. 48 (6), 610–631, doi: 10.1346/CCMN.2000.0480603.